Research Letter **DOI:** 10.15541/jim20250041

Boosting the Thermoelectric Performance of Full-Heusler Fe_2VAl Alloy *via* Substituting Al Site with V

ZHENG Yuanshun[1], YU Jian[2], YE Xianfeng[1], LIANG Dong[1], ZHU Wanting[1], NIE Xiaolei[1], WEI Ping[1], ZHAO Wenyu[1], ZHANG Qingjie[1]

(1. State Key Laboratory of Advanced Technology for Materials Synthesis and Processing, Wuhan University of Technology, Wuhan 430070, China; 2. School of Materials Science and Engineering, Jiujiang University, Jiujiang 332005, China)

Abstract: Full-Heusler Fe_2VAl alloy has received significant attention for thermoelectric (TE) applications due to its high mechanical strength, favorable electrical transport behavior, and earth-abundant constituent elements. However, its intrinsically high lattice thermal conductivity hinders the enhancement of the figure of merit (zT). In this study, a series of bulk materials with the nominal composition of $Fe_2V_{1+x}Al_{1-x}$ (x=0–0.21) were prepared by the arc-melting method. Effects of substituting Al site with V on the phase composition, microstructure, band structure, and TE transport properties were systematically investigated. All materials exhibit a single phase with a partially disordered B2 structure. V-doping shifts the Fermi level into the conduction band, significantly enhancing the carrier concentration, and resulting in a high power factor of 4.5 $mW\cdot K^{-2}\cdot m^{-1}$. Additionally, the lattice thermal conductivity is substantially reduced due to enhanced phonon scattering induced by the mass and stress fluctuations. Ultimately, a maximum zT of 0.14 is achieved for the material with x=0.15, which is nearly 280 times larger than that of undoped Fe_2VAl. This work demonstrates that substituting Al site with V can effectively improve the TE performance of Fe_2VAl alloy.

Key words: Fe_2VAl-based full-Heusler alloy; antisite defect; microstructure; thermoelectric performance

TE devices enable direct energy conversions between heat and electricity, presenting a scalable, reliable, and environmentally friendly solution for energy conversion applications such as waste-heat-energy harvesting[1]. The conversion efficiency predominantly depends on the performance of the TE material, which is typically evaluated by the dimensionless figure of merit $zT=\alpha^2\sigma T/\kappa$, where α, σ, T and κ denote the Seebeck coefficient, electrical conductivity, absolute temperature, and total thermal conductivity ($\kappa=\kappa_C+\kappa_L$, where κ_C is the electronic contribution and κ_L is the lattice contribution), respectively. An ideal TE material requires a high power factor ($\alpha^2\sigma$) and a low κ[2]. Over the past decades, substantial efforts have been made to enhance zT, primarily through band engineering for $\alpha^2\sigma$ optimization[3-5] and phonon engineering for κ_L reduction[6-7]. However, it is extremely difficult to boost zT due to the contradictorily coupled TE parameters, seriously hindering the large-scale application of TE materials[8].

Recently, full-Heusler alloys have received significant attention for TE applications owing to their earth-abundant, environmentally friendly constituent elements and robust mechanical strength, as well as remarkable thermal stability[9-10]. Ternary Fe_2VAl, as a typical semiconducting full-Heusler alloy, crystallizes in a fully ordered Cu_2MnAl-type $L2_1$ structure at low temperature, and transforms at ~1373 and ~1523 K into partially disordered CsCl-type B2 structure, and fully disordered W-type A2 structure[11-14], respectively, as sketched in Fig. 1(a). Fe_2VAl-based alloys usually exhibit excellent electrical properties due to the peculiar electronic structure, making them highly promising candidates for the prospective applications. Hinterleitner *et al*.[15] demonstrated that W-doped Fe_2VAl thin films achieved a

Received date: 2025-02-02; **Revised date:** 2025-04-13; **Published online:** 2025-04-27
Foundation item: National Natural Science Foundation of China (52130203, 92463310, 52201256); Guangdong Basic and Applied Basic Research Foundation (2022B1515120005)
Biography: ZHENG Yuanshun (1999–), male, Master candidate. E-mail: yszheng@whut.edu.cn
郑元顺(1999–), 男, 硕士研究生. E-mail: yszheng@whut.edu.cn
Corresponding author: YU Jian, associate professor. E-mail: yujian@jju.edu; ZHAO Wenyu, professor. E-mail: wyzhao@whut.edu.cn
余 健, 副教授. E-mail: yujian@jju.edu; 赵文俞, 教授. E-mail: wyzhao@whut.edu.cn

remarkable $\alpha^2\sigma$ of 400 μW·K^{-2}·cm^{-1}, an order of magnitude higher than Bi_2Te_3-based materials. However, the intrinsically high κ_L of Fe_2VAl pristine (~26 W·m^{-1}·K^{-1} at 300 K) severely constrains the enhancement of zT[13]. The recent studies have primarily focused on thermal transport optimization through enhanced phonon scattering mechanisms, including inducing the mass and stress fluctuations through atomic substitution[16], grain refining *via* high-pressure torsion[17] or ball milling[18], and inducing nanoscale precipitates *via* proper heat treatment[16]. The antisite defects[19], such as V_{Al}, Al_V in stoichiometric Fe_2VAl, and Fe_V, V_{Fe}, Fe_{Al}, Al_{Fe} in off-stoichiometric Fe_2VAl, can serve as electron donors or acceptors, and hence strongly influence the electronic transport properties. Miyazaki *et al*.[20] achieved a peak $\alpha^2\sigma$ of ~68 μW·K^{-2}·cm^{-1} at 300 K in n-type $Fe_2V_{1+x}Al_{1-x}$, and Diack-Rasselio *et al*.[21] reported a comparable value of ~67 μW·K^{-2}·cm^{-1} at 250 K for similar compositions. Recently, it was reported that the exceptional $\alpha^2\sigma$ of ~76 μW·K^{-2}·cm^{-1} can be obtained in undoped Fe_2VAl bulk *via* inducing a large amount of antisite defects by ultrafast quenching from elevated temperature[22]. These findings definitively validate that optimizing the antisite defect concentration is an effective strategy for enhancing TE performance in Fe_2VAl system.

In this study, we aimed to enhance the TE performance of full-Heusler Fe_2VAl alloy *via* optimizing the antisite defect V_{Al} concentration by substituting Al site with V. A series of bulk materials with the nominal composition of $Fe_2V_{1+x}Al_{1-x}$ (x=0–0.21) were prepared by the arc-melting method, and the effects of substituting Al site with V on the phase composition, microstructure, band structure, and thermoelectric transport properties were systematically investigated.

1 Experimental and theoretical methods

1.1 Preparation of materials

High-purity bulk Fe (99.99%), V (99.95%), and Al (99.99%) were weighed according to the nominal composition $Fe_2V_{1+x}Al_{1-x}$ (x=0, 0.03, 0.06, 0.09, 0.12, 0.15, 0.18, and 0.21). These elements were then arc-melted into ingots under an argon atmosphere. To ensure homogeneity, the ingots were subjected to five remelting cycles with intermediate flipping. The resultant ingots were designated as V00 to V21 according to their respective x. Using wire electrical discharge machining, the ingots were cut into rectangular bulks with dimensions of 3 mm×3 mm×13 mm and 8 mm×8 mm×1.8 mm, and circular slices with a diameter of 10 mm and a thickness of 1 mm, respectively. These specimens were used for characterizing the electrical transport properties, thermal transport properties, and Hall coefficient, respectively.

1.2 Characterization of material

The X-ray diffractometer (XRD, SmartLab, Rigaku Corporation, Japan) was employed to determine the phase composition using a Cu Kα radiation source with powders obtained by manually grinding the ingots in an agate mortar. The lattice parameters were refined according to the Rietveld method using the Fullprof program[23]. The electron probe micro-analyzer (EPMA, JXA-8230, Nippon Electronics Corporation, Japan) was utilized to characterize the microstructure and conduct elemental analysis.

1.3 Measurements of transport

The TE performance testing system (CTA, ZEM-3/500) was adopted to measure the electrical conductivity σ and the Seebeck coefficient α in a helium atmosphere within the temperature range from 300 to 800 K. The total thermal conductivity κ was calculated according to the formula $\kappa=\lambda\rho C_p$. Here, λ represents the thermal diffusivity measured by the laser thermal conductivity analyzer (LFA-467, NETZSCH), C_p is the specific heat capacity, which was calculated through the Dulong-Petit formula, and ρ is the bulk density measured by the Archimedes method. The Hall coefficient R_H was measured using a self-made instrument in a helium atmosphere. The carrier concentration n and Hall mobility μ were calculated based on the formulas $n=1/(eR_H)$ and $\mu=\sigma R_H$, where e is the elementary charge.

1.4 Computational method

The crystal structure optimization was carried out within the framework of density functional theory (DFT) and implemented in the Vienna *Ab initio* Simulation Package software[24]. The Perdew-Burke-Ernzerhof (PBE)[25] pseudopotential under the generalized gradient approximation and a Hubbard parameter U=3 eV were adopted as the exchange-correlation potential. The projected augmented wave (PAW) method was utilized to investigate the electron-ion interactions. The plane-wave cutoff energy for the optimization process was 500 eV, and a 7×7×7 Monkhorst-Pack k-mesh was employed. Considering the atomic and lattice relaxations, the Hellmann- Feynman forces between ions were lower than 0.0001 eV/Å, and the self-consistent energy of electrons was less than 10^{-7} eV.

2 Results and discussion

Fig. 1(b) shows powder XRD patterns of the $Fe_2V_{1+x}Al_{1-x}$ samples. It can be observed that the diffraction peaks of all samples match well with those of Fe_2VAl (JCPDS#01-073-8878), indicating a single-phase composition. It is worth noting that the (111) peak

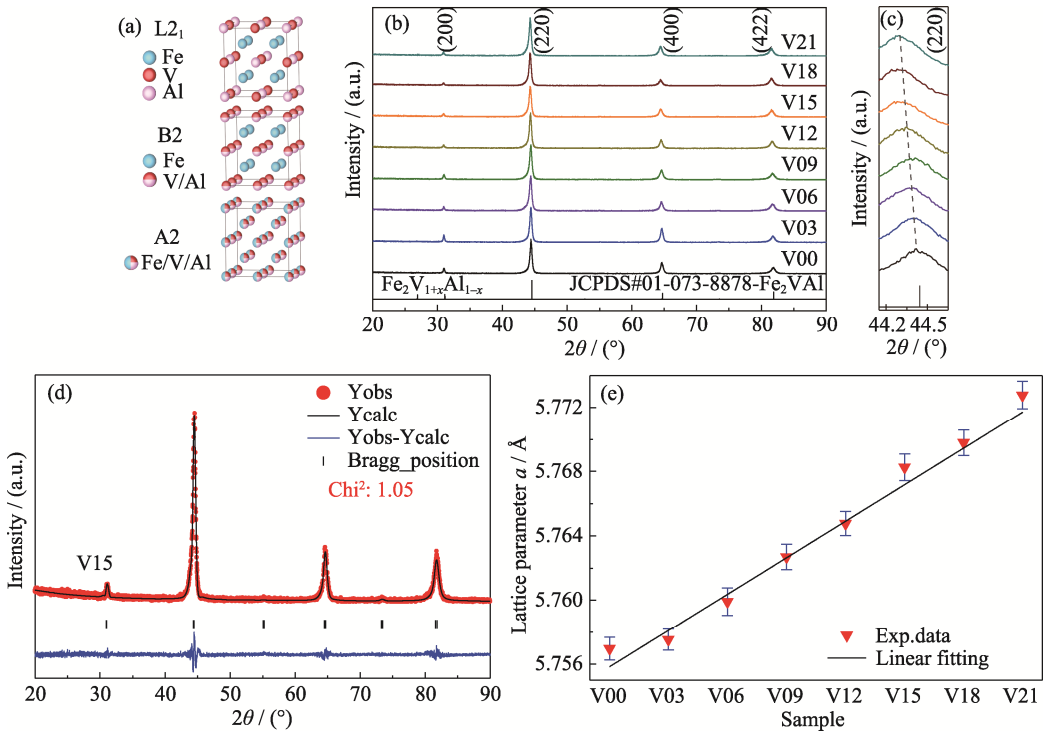

Fig. 1　Crystal structure and phase composition obtained from XRD analysis

(a) $L2_1$, B2, and A2 type crystal structures of Fe_2VAl; (b) Powder XRD patterns of all $Fe_2V_{1+x}Al_{1-x}$ materials; (c) Changes of the diffraction peak of (220) plane with the doping amount increasing; (d) XRD Rietveld refinement result of V15; (e) Lattice parameter of all $Fe_2V_{1+x}Al_{1-x}$ materials obtained through Rietveld refinement

completely disappears, while the (200) peak can be clearly observed, indicating the B2-type disorder between V and Al sites within all samples[10]. The strong disordering should originate mainly from two aspects. One is that V/Al antisite defects induced by high temperature were partly frozen by ultrafast cooling during the arc-melting process, and the other is microstrain introduced by manual grinding, which can also lead to disorder[26]. The enlarged XRD patterns, as depicted in Fig. 1(c), clearly reveal that the (220) diffraction peak gradually shifts to a lower angle with increasing V doping content, indicating a significant increase in the lattice constant. The lattice parameters of all samples were calculated based on the Rietveld method using the Fullprof software (Figs. 1(d, e)). The linear evolution of the lattice parameter is in good agreement with the literature reported by Diack-rasselio *et al*[21]. The increase in the lattice parameter can be explained by the charge transfer between atoms calculated through Bader charge analysis. In all $Fe_2V_{1+x}Al_{1-x}$ materials, both Al and V display a positive Bader charge, and $q_{Al}>q_V$, whereas Fe displays a negative Bader charge balance that satisfies the equation $2q_{Fe}+q_V+q_{Al}=0$, which implies a partial electron transfer from Al and V to Fe. When V substitutes Al, the Bader charge transfer from Al to both V and Fe causes expansion of their Bader volumes. This expansion, in turn, influences the bond lengths and bond angles between atoms, ultimately giving rise to an increase in the lattice parameter[27]. The continuous increase in lattice parameters with doping content also reveals that the solubility limit has not yet been achieved at the present doping amount.

Figs. 2(a-c) display the backscattered electron images of the polished surfaces of V00, V12 and V18 samples, respectively. Different shading was detected in all three samples. Nevertheless, the elemental mapping analysis of V18 sample, as shown in Figs. 2(d-f), indicates that all three constituent elements are uniformly distributed. Ten micro-regions for each sample were randomly selected to determine the actual composition by EDS. The results in Table 1 indicate that the actual V-doping contents are close to the nominal values. In addition, it is found that the microareas with different shading in each sample have nearly the same compositions, indicating the different shading actually originates from the different crystal orientations, which is consistent with the results reported in other literature[21].

To understand the impact of V doping on Fe_2VAl, band structure and total density of states (TDOS) calculations were performed on Fe_2VAl, $Fe_2V_{1.06}Al_{0.94}$ and $Fe_2V_{1.15}Al_{0.85}$, respectively, as shown in Fig. 3. The results indicate that Fe_2VAl is a direct bandgap semiconductor with a 0.12 eV gap, which is consistent with the measured results (0.1–0.2 eV) using photoconductivity

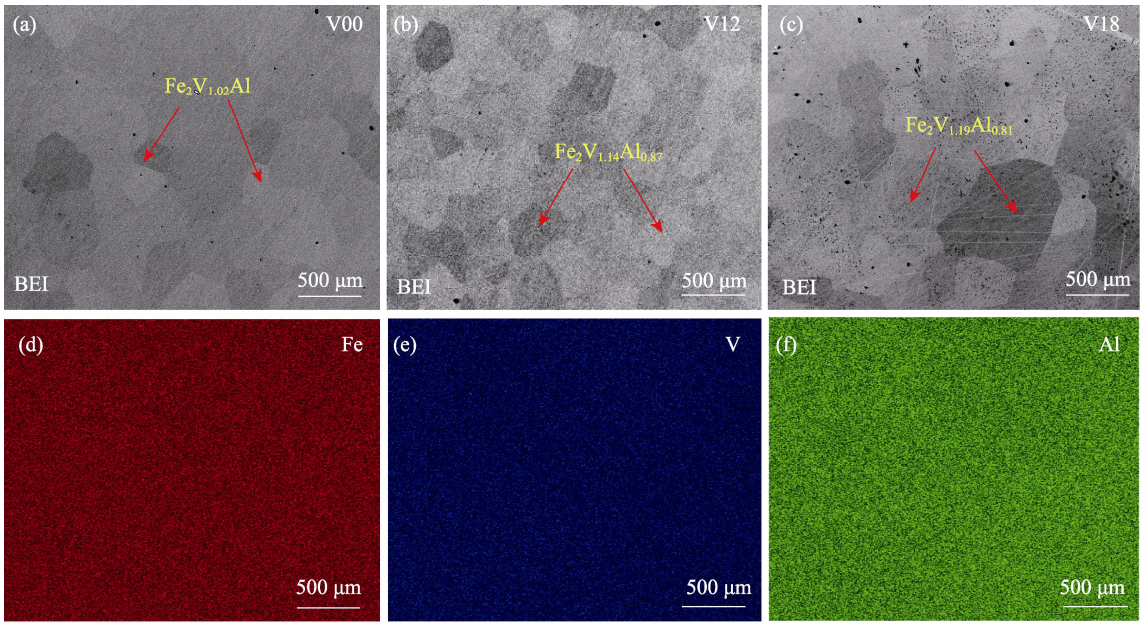

Fig. 2 Backscattered electron images and EDS mappings of selected $Fe_2V_{1+x}Al_{1-x}$ alloys
(a-c) Backscattered electron images of (a) V00, (b) V12, and (c) V18; (d-f) EDS elemental mappings of V18

Table 1 Nominal compositions, EDS-measured compositions, carrier concentrations, and carrier mobilities of $Fe_2V_{1+x}Al_{1-x}$ alloys at 300 K

Nom. Comp.	EDS Comp.	n/(×10^{20}, cm^{-3})	μ/(cm^2·V^{-1}·s^{-1})	Nom. Comp.	EDS Comp.	n/(×10^{20}, cm^{-3})	μ/(cm^2·V^{-1}·s^{-1})
Fe_2VAl	$Fe_2V_{1.02}Al$	3.5	11.5	$Fe_2V_{1.12}Al_{0.88}$	$Fe_2V_{1.14}Al_{0.87}$	−29.6	5.9
$Fe_2V_{1.03}Al_{0.97}$	$Fe_2V_{1.05}Al_{0.95}$	−10.0	10.1	$Fe_2V_{1.15}Al_{0.85}$	$Fe_2V_{1.16}Al_{0.82}$	−57.8	4.7
$Fe_2V_{1.06}Al_{0.94}$	$Fe_2V_{1.07}Al_{0.91}$	−13.7	13.4	$Fe_2V_{1.18}Al_{0.82}$	$Fe_2V_{1.19}Al_{0.81}$	−59.5	4.2
$Fe_2V_{1.09}Al_{0.91}$	$Fe_2V_{1.11}Al_{0.90}$	−35.5	3.8	$Fe_2V_{1.21}Al_{0.79}$	$Fe_2V_{1.24}Al_{0.77}$	−86.0	2.7

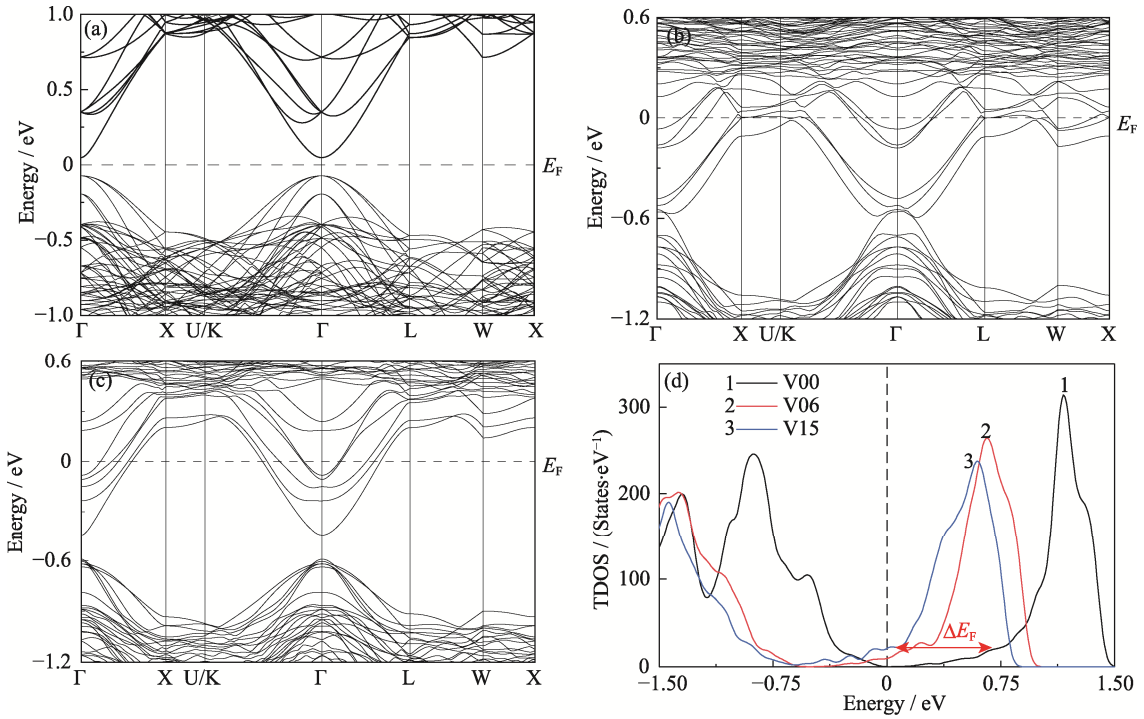

Fig. 3 Band structure and total density of states (TDOS) diagrams of the $Fe_2V_{1+x}Al_{1-x}$ alloys
(a-c) Energy band structure diagrams for (a) V00, (b) V06 and (c) V15; (d) Corresponding TDOS diagram showing the rigid band shift of the Fermi level caused by doping

measurements[28]. Besides, Nishino *et al*.[29] and Knapp *et al*.[30] also confirmed the non-metallic behavior of Fe_2VAl. After doping with V, the alloy gradually exhibits metallic properties, and the band gap gradually decreases to 0 eV, with the Fermi level E_F moving into the conduction band. This indicates that the V_{Al} antisite defects can serve as electron donors, which usually leads to a high carrier concentration and an enhanced electrical conductivity. Meanwhile, the rigid band-like displacement of E_F from the valence band edge to the conduction band enables a steep slope in the TDOS for $Fe_2V_{1.15}Al_{0.85}$. According to Mott's TE power theoretical formula (Equation (1))[15, 31]:

$$S(T) = -AT\frac{1}{N(E)}\frac{\partial N(E)}{\partial E}\bigg|_{E=E_F} \quad (1)$$

where A is a constant and T is the temperature. The absolute Seebeck coefficient is proportional to the logarithmic derivative of the density of states $N(E)$ with respect to energy at the E_F. The steep slope of TDOS suggests that the Seebeck coefficient may be significantly improved by V doping.

The room temperature carrier concentration and carrier mobility were measured, as shown in Table 1. n and μ of V00 are 3.5×10^{20} cm^{-3} and 11.5 $cm^2\cdot V^{-1}\cdot s^{-1}$, respectively, which are close to those reported by Garmroudi *et al*[22]. n increases significantly and μ decreases prominently as the V doping content increases. V21 has the highest $|n|$ of 8.6×10^{21} cm^{-3} and the lowest μ of 2.7 $cm^2\cdot V^{-1}\cdot s^{-1}$. The enhancement in n can be explained by the rigid band-like displacement of E_F from the valence band edge to the conduction band as mentioned above, and the reduction in μ is closely related to the enhanced carrier-carrier scattering.

Fig. 4 presents the temperature dependence of electrical conductivity σ, Seebeck coefficient α, and power factor $\alpha^2\sigma$ of all $Fe_2V_{1+x}Al_{1-x}$ materials. σ of the matrix V00 and V03 increases gradually with the temperature increasing, indicating the semiconducting characteristics. However, σ decreases with the temperature increasing when the V doping content exceeds 0.03, showing the typical metallic conduction characteristics. With the increase of the V doping content, σ firstly increases gradually due to the significantly enhanced n, and then slightly decreases from a doping content of 0.15 because of the deteriorated μ. The maximum σ reaching 4.4×10^5 S/m is obtained for V15, which increases nearly 6 times compared with the matrix Fe_2VAl. Fe_2VAl shows p-type semi-conduction at room temperature, and as the temperature increases, it exhibits a p-n transition due to the onset of intrinsic carrier excitation. After V doping, due to the rigid band-like displacement of E_F towards conduction band, the room temperature α exhibits a sign reversal, resulting in the majority of carriers changing from holes to electrons. Meanwhile, α significantly improves because of the steeper slope in TDOS as discussed above. V03 exhibits the highest α of –144.6 μV/K at 300 K. However, with a further increase of the doping content, α gradually decreases owing to the increased n. As a result, V06 sample shows the highest $\alpha^2\sigma$ reaching 4.5 $mW\cdot K^{-2}\cdot m^{-1}$ due to its good electrical conductivity and relatively high Seebeck coefficient, enhanced by two orders of magnitude compared to the matrix Fe_2VAl.

Fig. 5 shows the temperature dependence of thermal conductivity κ, carrier thermal conductivity κ_C and lattice thermal conductivity κ_L of $Fe_2V_{1+x}Al_{1-x}$ materials. κ of Fe_2VAl displays an extremely high value of 26.5 $W\cdot m^{-1}\cdot K^{-1}$ at 300 K. With V doping content of 0.21, κ is significantly reduced to about 10.9 $W\cdot m^{-1}\cdot K^{-1}$. κ_C was calculated according to the Wiedemann-Franz law[32]: $\kappa_C=L_0\sigma T$. Taking into account the influence of the intrinsic κ_C excitation of Fe_2VAl above 300 K, the Lorenz constant L_0 was calculated according to the equation $L_0 = 1.5 + \exp\left(-\frac{\alpha}{116}\right)$ proposed by Kim *et al*[33], where α is the Seebeck coefficient. κ_C increases significantly after doping with V, which is consistent with the changes of σ. κ_L of all the samples is estimated by κ–κ_C. κ_L decreases gradually due to the enhanced lattice vibration with the temperature increasing. After V doping, κ_L is

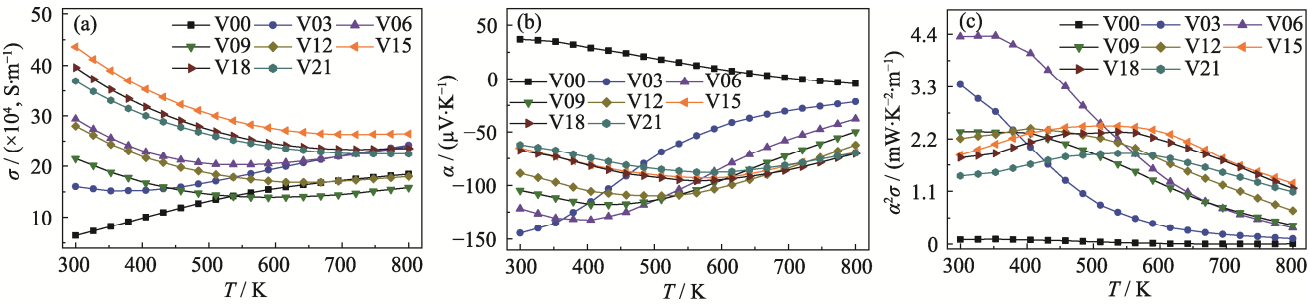

Fig. 4　Temperature dependence of (a) electrical conductivity, (b) Seebeck coefficient, and (c) power factor for all $Fe_2V_{1+x}Al_{1-x}$ materials in the temperature range of 300–800 K

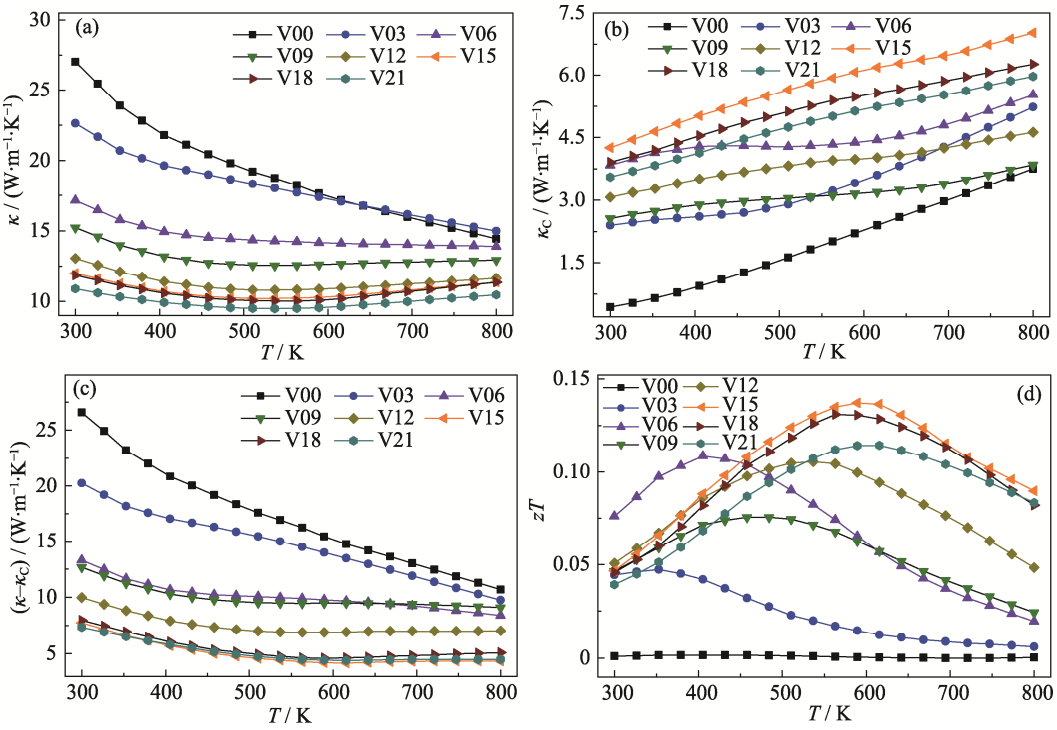

Fig. 5 Temperature dependence of (a) thermal conductivity, (b) electronic thermal conductivity, (c) lattice thermal conductivity, and (d) zT for all $Fe_2V_{1+x}Al_{1-x}$ alloys in the temperature range of 300–800 K

dramatically reduced due to the strong point-defect scattering induced by the mass and radius difference between V and Al atoms. V21 exhibits the low κ_L of 8.2 $W·m^{-1}·K^{-1}$ at 300 K and 6.1 $W·m^{-1}·K^{-1}$ at 800 K, reduced by 69.2% and 44% as compared to the matrix. zT values of all samples were calculated according to the formula $zT=\alpha^2\sigma T/\kappa$. Due to relatively high $\alpha^2\sigma$, V06 achieves a high zT value of 0.11 in the low-temperature region, which is approximately 70 times higher than that of Fe_2VAl. In the high-temperature region, V15 shows a peak zT of 0.14 at 590 K because of the low κ_L, which is approximately 280 times higher than that of Fe_2VAl. Although the obtained zT in this work is still relatively low as compared to other state-of-the-art TE materials, such as Bi_2Te_3 and SnSe, the excellent electrical properties and robust mechanical strength still make them as potential candidates for practical applications. Additionally, zT obtained in this work is significantly higher than those of the doped materials with rare earth elements at Al site, such as Ce (zT_{max}=0.030), Sm (zT_{max}=0.031), and Dy (zT_{max}=0.023)[12]. The main reason for the low zT is that the thermal conductivity remains at a relatively high level. Thus, it is advisable to consider co-doping other elements simultaneously to synergistically optimize the electrical and thermal transport properties. For instance, doping Nb at V site. According to the calculation results reported by Ye *et al*[34], Fe_2NbAl alloy may possess much lower κ compared to Fe_2VAl due to the strong crystal anharmonicity and higher $\alpha^2\sigma$ because of the high band degeneracy.

3 Conclusions

In summary, the effect of substituting Al site with V on the phase composition, microstructure, band structure, and TE transport properties of the full-Heusler alloy Fe_2VAl was systematically investigated. It was found that all doped materials exhibit the pure phase with a B2 structure. The electrical transport properties were effectively improved after V doping, and high $\alpha^2\sigma$ of 0.45 $mW·K^{-2}·m^{-1}$ was obtained, enhanced by two orders of magnitude compared to the Fe_2VAl matrix. Simultaneously, κ_L was substantially reduced because of the enhanced phonon scattering, and the lowest value of 6.1 $W·m^{-1}·K^{-1}$ was achieved. As a result, a peak zT of 0.14 was obtained at 590 K. This work demonstrates that substituting Al site with V can effectively improve the TE properties of the Fe_2VAl alloy.

References:

[1] YANG G S, SANG L A, ZHANG C, *et al*. The role of spin in thermoelectricity. *Nature Reviews Physics*, 2023, **5(8):** 466.

[2] KIM H S, LIU W S, REN Z F. The bridge between the materials and devices of thermoelectric power generators. *Energy & Environmental Science*, 2017, **10(1):** 69.

[3] PEI Y, SHI X, LALONDE A, *et al*. Convergence of electronic bands for high performance bulk thermoelectrics. *Nature*, 2011,

473(7345): 66.

[4] HEREMANS J P, JOVOVIC V, TOBERER E S, *et al*. Enhancement of thermoelectric efficiency in PbTe by distortion of the electronic density of states. *Science*, 2008, **321(5888):** 554.

[5] LABORATORY M, LIMITED D I, MIYUKIGAOKA. Improvement of the efficiency of thermoelectric energy conversion by utilizing potential barriers. *Japanese Journal of Applied Physics*, 1997, **36(1):** 170.

[6] ZHAO L D, LO S H, ZHANG Y, *et al*. Ultralow thermal conductivity and high thermoelectric figure of merit in SnSe crystals. *Nature*, 2014, **508(7496):** 373.

[7] LAN Y C, MINNICH A J, CHEN G, *et al*. Enhancement of thermoelectric figure-of-merit by a bulk nanostructuring approach. *Advanced Functional Materials*, 2010, **20(3):** 357.

[8] MAHAN G D, SOFO J O. The best thermoelectric. *Proceedings of the National Academy of Sciences of the United States of America*, 1996, **93(15):** 7436.

[9] TAVARES S S, YANG K S, MEYERS M A. Heusler alloys: past, properties, new alloys, and prospects. *Progress in Materials Science*, 2023, **137:** 101017.

[10] GRAF T, FELSER C, PARKIN S S P. Simple rules for the understanding of Heusler compounds. *Progress in Solid State Chemistry*, 2011, **39(1):** 1.

[11] VAN DER REST C, DUPONT V, ERAUW J P, *et al*. On the reactive sintering of Heusler Fe_2VAl-based thermoelectric compounds. *Intermetallics*, 2020, **125:** 106890.

[12] HARI S R, SRINIVAS V, LI C R, *et al*. Thermoelectric properties of rare-earth doped Fe_2VAl Heusler alloys. *Journal of Physics-Condensed Matter*, 2020, **32(35):** 355706.

[13] KAWAHARADA Y, KUROSAKI K. Thermophysical properties of Fe_2VAl. *Journal of Alloys and Compounds*, 2003, **352(1/2):** 48.

[14] SHAMIM S K, DEVI P, SINGH S, *et al*. Thermoelectric properties of Fe_2VAl in the temperature range 300–800 K: a combined experimental and theoretical study. *Physica B-Condensed Matter*, 2024, **673:** 415496.

[15] HINTERLEITNER B, KNAPP I, PONEDER M, *et al*. Thermoelectric performance of a metastable thin-film Heusler alloy. *Nature*, 2019, **576(7785):** 85.

[16] GARMROUDI F, PARZER M, RISS A, *et al*. Solubility limit and annealing effects on the microstructure & thermoelectric properties of $Fe_2V_{1-x}Ta_xAl_{1-y}Si_y$ Heusler compounds. *Acta Materialia*, 2021, **212:** 116867.

[17] FUKUTA K, TSUCHIYA K, MIYAZAKI H, *et al*. Improving thermoelectric performance of Fe_2VAl-based Heusler compounds *via* high-pressure torsion. *Applied Physics A: Materials Science & Processing*, 2022, **128(3):** 184.

[18] ALLENO E. Review of the thermoelectric properties in nanostructured Fe_2VAl. *Metals*, 2018, **8(11):** 864.

[19] ALLENO E, DIACK-RASSELIO A, NOUTACK M S T. Optimization of the thermoelectric properties in self-substituted Fe_2VAl. *Physical Review Materials*, 2023, **7(7):** 075403.

[20] MIYAZAKI H, TANAKA S, IDE N, *et al*. Thermoelectric properties of Heusler-type off-stoichiometric $Fe_2V_{1+x}Al_{1-x}$ alloys. *Materials Research Express*, 2014, **1(1):** 015901.

[21] DIACK-RASSELIO A, ROULEAU O, COULOMB L, *et al*. Influence of self-substitution on the thermoelectric Fe_2VAl Heusler alloy. *Journal of Alloys and Compounds*, 2022, **920:** 166037.

[22] GARMROUDI F, PARZER M, RISS A, *et al*. Anderson transition in stoichiometric Fe_2VAl: high thermoelectric performance from impurity bands. *Nature Communications*, 2022, **13:** 3599.

[23] CUI X, FENG Z, JIN Y. AutoFP: a GUI for highly automated Rietveld refinement using an expert system algorithm based on FullProf. *Journal of Applied Crystallography*, 2015, **48(5):** 1581.

[24] PERDEW J P, RUZSINSZKY A, CSONKA G I, *et al*. Exchange and correlation in open systems of fluctuating electron number. *Physical Review A*, 2007, **76(4):** 040501.

[25] SHAM L J, KOHN W. One-particle properties of an inhomogeneous interacting electron gas. *Physical Review B*, 1966, **145(2):** 561.

[26] MAIER S, DENIS S, ADAM S, *et al*. Order-disorder transitions in the Fe_2VAl Heusler alloy. *Acta Materialia*, 2016, **121:** 126.

[27] HINTERLEITNER B, GARMROUDI F, REUMANN N, *et al*. The electronic pseudo band gap states and electronic transport of the full-Heusler compound Fe_2VAl. *Journal of Materials Chemistry C*, 2021, **9(6):** 2073.

[28] OKAMURA H, KAWAHARA J, NANBA T, *et al*. Pseudogap formation in the intermetallic compounds $(Fe_{1-x}V_x)_3Al$. *Physical Review Letters*, 2000, **84(16):** 3674.

[29] NISHINO Y, KATO M, ASANO S, *et al*. Semiconductor-like behavior of electrical resistivity in Heusler-type Fe_2VAl compound. *Physical Review Letters*, 1997, **79(10):** 1909.

[30] KNAPP I, BUDINSKA B, MILOSAVLJEVIC D, *et al*. Impurity band effects on transport and thermoelectric properties of $Fe_{2-x}Ni_xVAl$. *Physical Review B*, 2017, **96(4):** 045204.

[31] GARMROUDI F, RUSS A, PARZER M, *et al*. Boosting the thermoelectric performance of Fe_2VAl-type Heusler compounds by band engineering. *Physical Review B*, 2021, **103(8):** 085202.

[32] SHIN W H, ROH J W, RYU B, *et al*. Enhancing thermoelectric performances of bismuth antimony telluride *via* synergistic combination of multiscale structuring and band alignment by $FeTe_2$ Incorporation. *ACS Applied Materials & Interfaces*, 2018, **10(4):** 3689.

[33] KIM H S, GIBBS Z M, TANG Y L. Characterization of Lorenz number with Seebeck coefficient measurement. *APL Materials*, 2015, **3(4):** 041506.

[34] YE X F, YU J, KE S Q, *et al*. Excellent thermoelectric performance of Fe_2NbAl alloy induced by strong crystal anharmonicity and high band degeneracy. *npj Quantum Materials*, 2024, **9(1):** 60.

V 取代 Al 位提升全赫斯勒合金 Fe_2VAl 的热电性能

郑元顺[1], 余 健[2], 叶先峰[1], 梁 栋[1], 朱婉婷[1],
聂晓蕾[1], 魏 平[1], 赵文俞[1], 张清杰[1]

(1. 武汉理工大学 材料复合新技术国家重点实验室, 武汉 430070; 2. 九江学院 材料科学与工程学院, 九江 332005)

摘 要: 全赫斯勒合金 Fe_2VAl 具有机械强度较高、电输运性能好和组成元素地球丰度高的优势, 在热电领域受到广泛关注。然而, 该合金的高晶格热导率极大限制了热电优值(zT)的提升。本研究采用电弧熔炼法制备了一系列名义化学成分为 $Fe_2V_{1+x}Al_{1-x}$(x=0~0.21)的块体材料, 系统研究了 V 取代 Al 位对物相组成、显微结构、能带结构和热电输运性能的影响。结果表明, 所有材料均为部分无序的 B2 单相结构。V 掺杂可将费米能级上移至导带, 大幅度增大载流子浓度, 并将功率因子提升至 4.5 $mW\cdot K^{-2}\cdot m^{-1}$。同时, 由于质量与应力波动引起的声子散射作用增强, 晶格热导率显著降低。最终, x=0.15 的材料的最大 zT 达到 0.14, 与未掺杂 Fe_2VAl 材料相比提升近 280 倍。该研究表明 V 取代 Al 位可以有效提升 Fe_2VAl 合金的热电性能。

关 键 词: Fe_2VAl 基全赫斯勒合金; 反位缺陷; 显微结构; 热电性能

中图分类号: TB34 **文献标志码:** A **文章编号:** 1000-324X(2025)12-1425-08